

COMMISSIONING THE 400-MeV LINAC AT J-PARC AND HIGH INTENSITY OPERATION OF THE J-PARC RCS

Hideaki Hotchi^{#,1)} and J-PARC beam commissioning team^{1), 2)}

¹⁾ J-PARC, JAEA, Tokai, Naka, Ibaraki, 319-1195 Japan

²⁾ J-PARC, KEK, Oho, Tsukuba, Ibaraki, 305-0801 Japan

Abstract

In the summer shutdown of 2013, the output energy of the J-PARC linac was upgraded from 181 MeV to the design value of 400 MeV. With this upgraded injection energy, the following RCS successfully demonstrated 550-kW high intense acceleration at a low-level beam loss. The main topic of this paper is to discuss the outcome of the recent high intensity beam tests in the RCS, mainly focusing on our approach to beam loss issues.

INTRODUCTION

The J-PARC is a multi-purpose proton accelerator facility aiming at MW-class output beam power, which comprises a chain of three accelerators (a 400-MeV H⁻ linac, a 3-GeV rapid cycling synchrotron; RCS, and a 50-GeV main ring synchrotron; MR) and three experimental facilities (a materials and life science experimental facility; MLF, a hadron experimental facility; HD, and a neutrino experimental facility; NU).

In the summer shutdown of 2013, the output energy of the linac was upgraded from 181 MeV to the design value of 400 MeV. Thus now the linac and the following RCS are in the new phase to further ramp up the output beam power toward its design value of 1 MW from the RCS. In this paper, we present the outcome of the recent high intensity beam trial performed in the RCS before and after the linac energy upgrade, together with the brief report on the beam commissioning status of the linac.

OUTLINE OF THE LINAC AND RCS, AND THEIR OPERATIONAL HISTORY

The linac consists of an H⁻ ion source (IS), a radio frequency quadrupole linac (RFQ), a drift tube linac (DTL) and a separate-type DTL (SDTL). In addition, in the summer shutdown of 2013, an annular-ring coupled structure (ACS) linac [1] was installed, by which the output energy of the linac was upgraded from 181 MeV to the design value of 400 MeV. In addition, in the next summer shutdown of 2014, the front-end system (IS and RFQ) will be replaced, by which the peak current is to be increased from 30 mA to the design value of 50 mA. By this improvement, the output beam power from the linac will be increased to the design value of 133 kW.

The 400-MeV H⁻ beam from the linac is delivered to the RCS injection point, where it is multi-turn charge-exchange injected through a carbon stripper foil over a period of 0.5 ms. The RCS accelerates the injected protons up to 3 GeV with a repetition rate of 25 Hz,

providing the 3-GeV proton beam both to MLF and MR. At the current capability of the linac, the RCS can produce 600 kW output beam power, which will be increased to the design value of 1 MW following the peak current upgrade of the linac in this summer.

The J-PARC beam commissioning began in November 2006 from the linac [2]. Then the RCS was beam commissioned in October 2007 [3-4]. Following the initial beam tuning and underlying beam tests, the linac and RCS started up the user program with a low power beam of 4 kW in December 2008. Fig. 1 shows the history of the linac and RCS beam operation. As shown in the figure, the output beam power has been steadily increasing following the progression in beam tuning and hardware improvements [5-6]. Before upgrading the linac energy, we achieved 300-kW routine beam operation. After completing the ACS installation and their in-situ high power test, we started beam commissioning of the linac in December 2013 and then the RCS in January 2014. Via the initial beam tuning, the linac and RCS resumed the user program in February 2014 with an output beam power of 300 kW.

In parallel with the routine user run, we have been intermittently continuing the high intensity beam tests. So far, the RCS has successfully achieved high intensity beam trials of up to 550 kW for both injection energies of 181 MeV and 400 MeV.

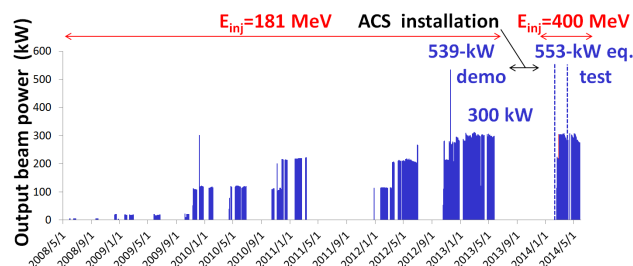


Figure 1: Beam operational history of the linac and RCS since the start-up of the user program.

BEAM COMMISSIONING STATUS OF THE 400-MeV LINAC

The 400-MeV linac started beam commissioning on December 16, 2013, and then successfully established 400-MeV acceleration on January 17, 2014 as planned. Via the initial beam tuning, the linac started beam delivery to the RCS on January 30 for their beam commissioning with the injection energy of 400 MeV.

Fig. 2 shows the beam profiles measured for $I_{\text{peak}}=25$ mA at the entrance (191 MeV) and exit (400 MeV) of the ACS. As shown in the figure, significant beam halo

hotchi.hideaki@jaea.go.jp

Any distribution of this work must maintain attribution to the author(s), title of the work, publisher, and DOI.

formation was observed downstream of the ACS. The most probable cause of this beam halo formation is a longitudinal mismatch at the ACS section. It leads to transverse-longitudinal motion coupling through space charge, causing beam emittance growth. In order to remove the longitudinal mismatch, we are to install bunch shape monitors (BSM) in the summer shutdown period of 2014. Longitudinal matching with BSMs will be performed in October 2014 after the summer shutdown.

In addition, similar emittance growth was found downstream of the second debuncher (DB2) installed in the beam transport line between the linac and the RCS. The main cause of this emittance growth is an over-focus of the longitudinal bunch by the DB2. Now the DB2 operates to defocus the momentum spread following the requirement from the RCS, while it also acts to focus the longitudinal bunch. In order to suppress the extra emittance growth, we will try re-optimization of the DB2 parameter in the next beam study period.

Though there remain some issues in beam tuning, the 400-MeV linac was successfully beam commissioned as planned, and is now stably delivering the 400-MeV beam to the RCS.

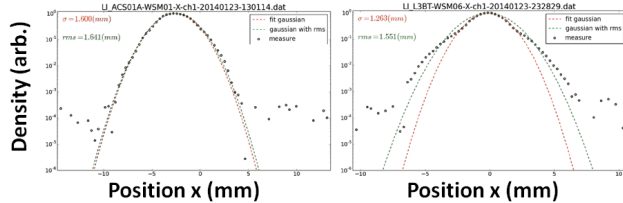


Figure 2: Beam profiles measured for $I_{\text{peak}}=25$ mA at the entrance (left) and exit (right) of the ACS.

HIGH INTENSITY BEAM TRIALS OF UP TO 550 kW IN THE RCS

After commissioning the linac, the RCS started beam tuning for the upgraded injection energy of 400 MeV on January 30, 2014. The initial beam tuning was rapidly completed by optimizing the use of the first 10 days. Then we performed a high intensity beam trial of up to 550 kW using a 0.5 ms-long linac pulse with a peak current of 24.6 mA and a chopper beam-on duty factor of 60%. In this experiment, the operating point was set at (6.45, 6.42), where we performed systematic beam loss measurements for various operational parameters and beam intensities. In this section, these experimental results are presented, and compared with the old data taken for the lower injection energy of 181 MeV and also with the corresponding numerical simulation results.

Painting Parameter Dependence of Beam Loss

In order to minimize space-charge induced beam loss at the low energy, the RCS employs injection painting both for the transverse and longitudinal phase spaces [7]. On the transverse plane, correlated painting with a painting emittance of 100π mm mrad (ϵ_{tp}) was applied in this beam test. On the other hand, for longitudinal painting [8-9], the momentum offset injection of 0.0, -0.1 and -0.2%

($\Delta p/p$) was tested in combination with superposing a second harmonic rf with an amplitude of 80% (V_2/V_1) of the fundamental rf. As an additional control in longitudinal painting, the phase sweep of the second harmonic rf was employed during injection from -100 to 0 degrees (ϕ_2) relative to the fundamental rf. With the systematic combinations of transverse and longitudinal painting listed in Table 1, we performed beam loss measurements.

Table 1: Painting Parameters Applied in The Beam Test

Parameter ID	ϵ_{tp} (π mm mrad)	V_2/V_1 (%)	ϕ_2 (degrees)	$\Delta p/p$ (%)
1	—	—	—	—
2	100	—	—	—
3	—	80	-100	—
4	—	80	-100	-0.1
5	—	80	-100	-0.2
6	100	80	-100	—
7	100	80	-100	-0.1
8	100	80	-100	-0.2

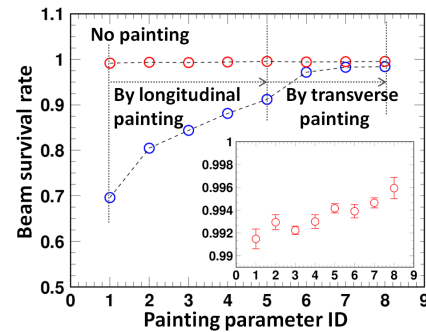


Figure 3: Beam survival rates measured for the painting parameter IDs 1 to 8 listed in Table 1, where the red circles correspond to the data taken for $E_{\text{inj}}=400$ MeV and $W_{\text{ext}}=550$ kW, while the blue ones are for $E_{\text{inj}}=181$ MeV and $W_{\text{ext}}=540$ kW.

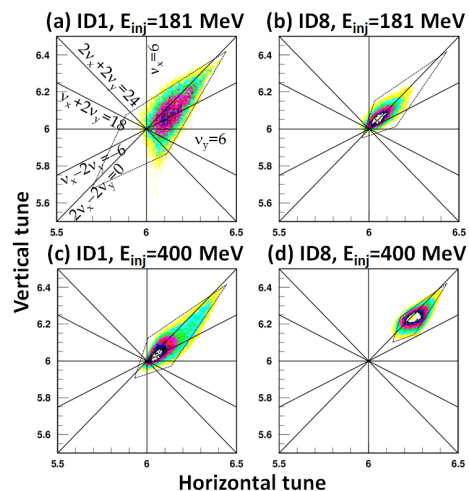


Figure 4: Tune footprints calculated at the end of injection for $E_{\text{inj}}=181$ MeV and $W_{\text{ext}}=540$ kW (upper) and for $E_{\text{inj}}=400$ MeV and $W_{\text{ext}}=550$ kW (lower), without (ID 1) and with (ID 8) injection painting.

Figure 3 shows beam survival rates measured for the painting parameter IDs 1 to 8, where the red circles correspond to the data taken for the injection energy of $E_{inj}=400$ MeV with a beam intensity of $W_{ext}=550$ kW (4.6×10^{13} ppp), while the blue ones are for $E_{inj}=181$ MeV and $W_{ext}=540$ kW (4.5×10^{13} ppp).

The larger painting parameter dependence was observed for $E_{inj}=181$ MeV, since the space-charge effect is more critical. For the case with no painting, 30%-big beam loss appeared. But this beam loss was drastically decreased from ID 1 to ID 5 by longitudinal painting, and from ID 5 to ID 8 by adding transverse painting. The plots (a) and (b) in Fig. 4 show tune footprints calculated at the end of injection for $E_{inj}=181$ MeV and $W_{ext}=540$ kW without and with injection painting. As shown in the plot (a), a core part of the beam particles crosses various low-order systematic resonances in the case with no painting. Such particles on the resonances suffer from emittance dilutions. This is the main cause of the 30%-big beam loss. Injection painting well decreases the space-charge tune depression as shown in the plot (b), leading to the significant beam loss mitigation from ID 1 to ID 8.

The beam survival was still improved for $E_{inj}=400$ MeV, as shown by the red circles in Fig. 3. This reflects the further space-charge mitigation by the higher injection energy as per the $\beta^2\gamma^3$ scaling law, as shown by the comparison of the upper plots and the lower ones in Fig. 4. The more clear painting parameter dependence can be confirmed by the inset in Fig. 3, which has a similar dependence to that for $E_{inj}=181$ MeV. This experimental data most clearly shows the enormous gain from the injection energy upgrade this time, as well as the excellent ability of injection painting.

Time Structure of Beam Loss

Figure 5 shows the beam loss monitor signals at the collimator section measured with the painting parameter ID 8 for $E_{inj}=181$ MeV and $W_{ext}=540$ kW and for $E_{inj}=400$ MeV and $W_{ext}=550$ kW. As shown in the figure, the beam loss appears only for the first 5 ms at the low energy.

In the data for $E_{inj}=181$ MeV, we can see characteristic two peak structures of beam loss. The first peak structure is mainly from foil scattering during injection. This part of beam loss was mitigated for $E_{inj}=400$ MeV, because the angular distribution of foil scattering shrinks for the higher injection energy due to the Lorentz boost.

On the other hand, the second peak structure of beam loss observed for $E_{inj}=181$ MeV arises from a dipole field ripple. In the RCS, beam injection is performed with four sets of pulse-type injection bump magnets, in which the rf-shielded ceramics chambers are installed. The source of the dipole field ripple is resonant currents in the rf shield loop (red loop in Fig. 6) induced by the $\Delta B/\Delta t$ of the injection bump field [10]. If the rf-shield keeps a symmetric configuration, the dipole field ripple can be cancelled out through the four injection bump magnets. But the symmetric condition was then out of order, since a part of capacitors was broken by the injection bump field because of the lack of their withstand voltage. The dipole

ripple component left due to such an asymmetric configuration affected the beam. The left plot in Fig. 7 shows the time structure of kick angle of the dipole field ripple estimated from the beam position data. The dipole field ripple appears only for the first 1 ms when the injection bump is active, and its frequency is 100 kHz which corresponds to 0.2 in tune.

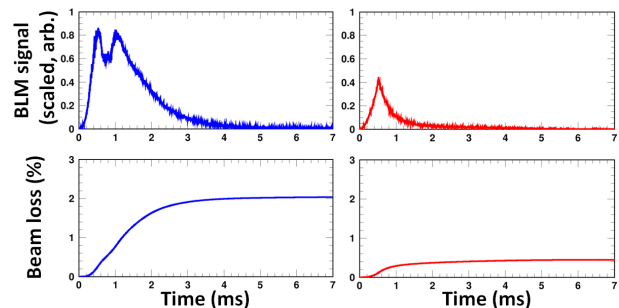


Figure 5: [Top] Scintillation-type beam loss monitor signals at the collimator measured with the painting parameter ID 8 for $E_{inj}=181$ MeV and $W_{ext}=540$ kW (left) and for $E_{inj}=400$ MeV and $W_{ext}=550$ kW (right). [Bottom] Beam loss estimated from the integration of the beam loss monitor signal.

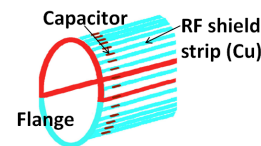


Figure 6: Schematic of the rf-shielded ceramics chamber installed in four sets of the injection bump magnets.

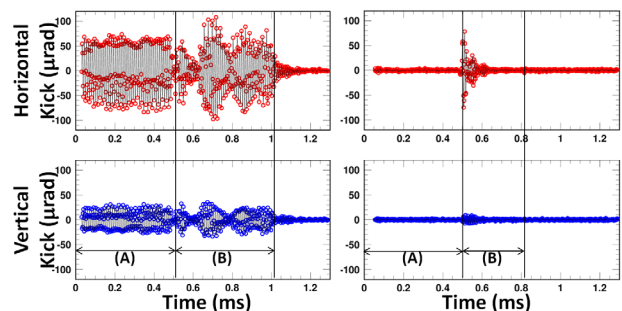


Figure 7: Time structure of kick angle of the dipole field ripple before (left) and after (right) the measures, estimated from the beam position data, where the region (A) corresponds to the flattop of the injection bump, while the region (B) is its fall time.

Recently the power supply of the injection bump magnets (based on the IGBT chopping system) was replaced to a new one (based on the pulse forming network system by capacitors) to match $E_{inj}=400$ MeV [11], by which the ripple component of the injection bump field itself was drastically reduced. Namely the driving force to excite the resonant currents in the rf shield loop was reduced. In addition, the rf shield itself was repaired using new capacitors with the higher withstand voltage. The more symmetric configuration of

Content from this work may be used under the terms of the CC BY 3.0 licence (© 2014). Any distribution of this work must maintain attribution to the author(s), title of the work, publisher, and DOI.

the repaired rf shield acts to well compensate the dipole field ripple. As shown in the right plot in Fig. 7, the dipole ripple was drastically reduced after these hardware improvements. This is the reason of the significant mitigation of the second peak structure of beam loss achieved for $E_{inj}=400$ MeV.

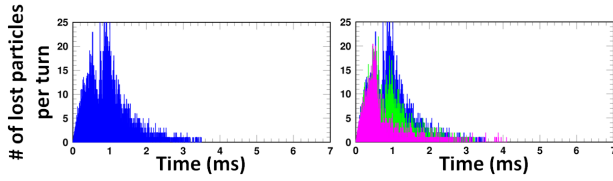


Figure 8: [Blue] Beam loss calculated with the painting parameter ID 8 for $E_{inj}=181$ MeV and $W_{ext}=540$ kW. [Right-green] Similar result calculated with $\rho=0.290$ m (two times larger pipe radius). [Right-pink] Similar one calculated simply with no dipole field ripple.

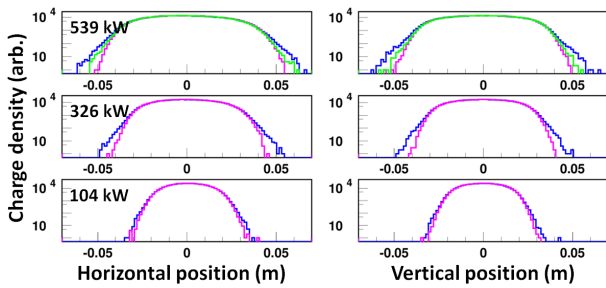


Figure 9: [Top] Beam profile calculated at the end of injection with the painting parameter ID 8 for $E_{inj}=181$ MeV and $W_{ext}=540$ kW without (pink) and with (blue) the dipole field ripple, where the green curves show another result calculated with $\rho=0.290$ m including the dipole field ripple. [Middle and bottom] Intensity dependence of beam halo formation caused by the dipole field ripple.

Consideration for the Beam Loss Mechanism Caused by the 100-kHz Dipole Field Ripple

Here we will discuss a more detailed mechanism of the beam loss caused by the 100-kHz dipole field ripple.

As shown by the left plot in Fig. 8, the numerical simulation well reproduces the measured time structure of beam loss given in the left plot of Fig. 5. The top plot of Fig. 9 shows the corresponding beam profiles calculated at the end of injection without and with the dipole field ripple. As shown in the plot, the dipole field ripple makes the emittance growth from pink to blue. In addition, its intensity dependence can be found in the same figure; the larger emittance growth appears for the higher intensity beam. Also this emittance growth has dependence on the radius of the beam pipe as shown in the top plot of Fig. 9; the emittance growth is mitigated from blue to green for the larger beam pipe radius. As shown in the right plot in Fig. 8, the second peak structure of beam loss is correspondingly mitigated from blue to green for the larger beam pipe radius.

These numerical simulation results imply that the beam loss caused by the dipole field ripple arises from the

combined effect of the coherent beam position oscillation and the image charge. The following two equations of motion express the coherent (1) and incoherent (2) motions of beam particles,

$$\bar{\chi}'' + k(s)\bar{\chi} = f(\theta, t) + \frac{2r_p\lambda}{e\beta^2\gamma\rho^2}\bar{\chi} + \dots(1)$$

$$(\chi_i - \bar{\chi})'' + k(s)(\chi_i - \bar{\chi}) = \sum_j F_{sc\ ij} + \frac{2r_p\lambda}{e\beta^2\gamma\rho^4}(\chi_i - \bar{\chi})^2 + \dots(2)$$

where “ $F_{sc\ ij}$ ” is the space charge among particles, “ f ” is the dipole field ripple, and the second term on the right side in each equation arises from the image charge. The image charge force contributing to the incoherent motion is a focusing force, of which the characteristic feature is to be proportional to the square of the coherent beam position. Therefore this focusing force can excite a beam envelope oscillation with 2 times higher frequency than that of the coherent beam position oscillation and can be a source of half-integer resonance of $2\nu=0.4$. Also this force depends on the beam intensity (λ) and the beam pipe radius (ρ). More detailed analysis is necessary to get the conclusion, but it seems this is the most probable driving force for the emittance growth and its resultant beam loss caused by the 100-kHz dipole field ripple.

Intensity Dependence of Beam Loss Measured for the Injection Energy of 400 MeV

The next topic is the beam intensity dependence of beam loss measured for $E_{inj}=400$ MeV with the painting parameter ID 8. In this measurement, the beam intensity was varied from 100 kW to 550 kW by thinning the number of intermediate pulses while keeping the injection pulse length of 0.5 ms. This type of intensity variation does not change the condition of injection painting and also does not change the foil hitting rate during injection.

The left-top plot of Fig. 10 shows beam loss monitor signals measured for $W_{ext}=100$ kW~550 kW. As shown in the figure, the beam losses for all the cases appear only for the first a few ms in the low energy region. The intensity dependence of beam loss amount estimated from the integration of the beam loss monitor signal is shown in the left-bottom plot of Fig. 10. Though the beam loss powers for all the cases are still much less than the beam loss limit of 4 kW (collimator capability) in the RCS, there is a possibility to further reduce the beam loss. As shown in the left-bottom plot, the beam loss amount has a linear response up to $W_{ext}=400$ kW, but the extra beam loss increase was observed for $W_{ext}=550$ kW. This means the beam loss of up to $W_{ext}=400$ kW is well minimized, which is only from the foil scattering during injection, but the beam loss observed for $W_{ext}=550$ kW still includes extra component other than the foil scattering beam loss.

As shown in the right plot in Fig. 10, this intensity dependence of beam loss is well reproduced by the corresponding numerical simulation. Fig. 11 shows transverse injection painting area estimated from the measured property of the injection beam. In this beam test, 100π -mm-mrad transverse painting was applied. In this figure, the black solid ellipse shows the design painting

area of 100π mm mrad, which is formed from the design beam emittance and Twiss parameter of the injection beam. But now the injection beam has a relatively large beam tail component as already mentioned. In addition, its Twiss parameter at the injection point has not been adjusted yet. Such a remaining beam halo component and Twiss parameter mismatch of the injection beam deviates the painting area and form terribly large emittance beam particles during the injection painting process as shown by the red solid ellipse in Fig. 11. The numerical simulation implies that such large amplitude particles cause the extra beam loss observed for $W_{\text{ext}}=550$ kW.

In order to reduce the extra beam loss, we will try beam tuning for the injection beam in the next beam study period scheduled at the end of June, 2014.

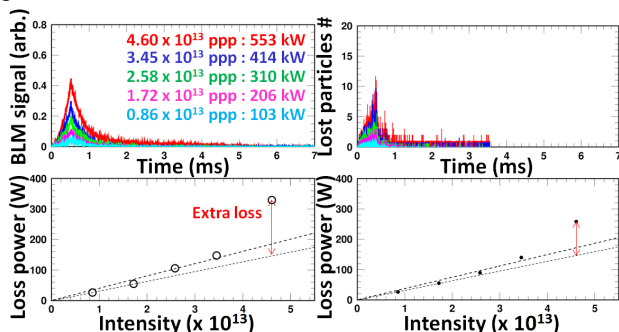


Figure 10: [Left-top] Intensity dependence of beam loss monitor signals measured with the painting parameter ID 8 for $E_{\text{inj}}=400$ MeV. [Left-bottom] Intensity dependence of beam loss amount estimated from the integration of the beam loss monitor signal. [Right] Corresponding numerical simulation results.

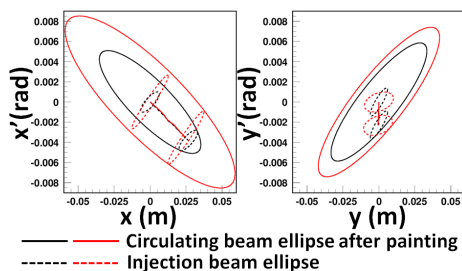


Figure 11: Transverse painting area, where the black ellipses show the design painting process with a painting emittance of 100π mm mrad, while the red ones show the actual painting process evaluated from the measured property of the injection beam.

NUMERICAL SIMULATION FOR THE 1-MW BEAM OPERATION OF THE RCS

Figure 12 shows the beam loss expected for the 1-MW design beam operation of the RCS. The left plot shows the beam loss calculated with all the imperfections including the present quality of the injection beam. Namely the injection beam has around 2 times larger beam emittance and remains a Twiss parameter mismatch. In this case, the beam loss was estimated to be

0.55% which corresponds to 733 W in power. The right plot is a similar result calculated with the design injection beam. In this case, the beam loss was well minimized to be 0.2% which is only from foil scattering. The beam losses for both cases are still much less than the current beam loss limit of 4 kW. The latest numerical simulation gives the positive result for the coming 1-MW design beam operation, but also implies that the quality of the injection beam is a key to minimize its beam loss.

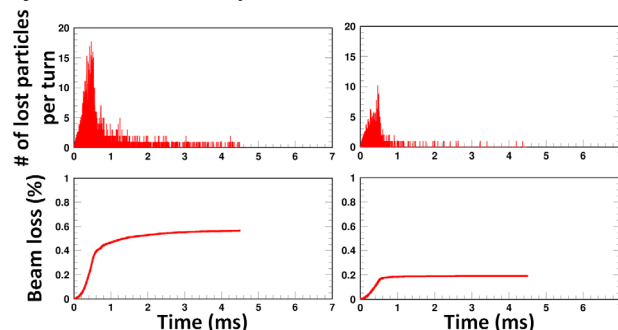


Figure 12: Expected beam loss for the 1-MW design beam operation of the RCS, where the left plot shows the beam loss calculated with all the imperfections including the present quality of the injection beam, while the right plot is the similar result with the design injection beam.

SUMMARY AND FUTURE PLAN

The 400-MeV linac was successfully commissioned as planned, and then the following RCS also rapidly achieved 3-GeV acceleration with the upgraded injection energy of 400 MeV. Via the initial beam tuning, the RCS performed high intensity beam tests, in which we confirmed the big gain from the injection energy upgrade this time and successfully demonstrated 550-kW-eq. high intense beam acceleration at a low-level beam loss of less than 0.5%. The linac and RCS have been stably delivering the 300-kW beam since the re-startup of the user program. Its beam power will be increased to >500 kW after replacing the neutron target at the MLF in this summer.

In the beam commissioning period from December 2013, a lot of useful data was taken toward realizing the 1-MW design beam operation. The 1-MW beam tuning is to start in October 2014 after replacing the front-end system of the linac in this summer.

REFERENCES

- [1] H. Ao et al., PRST-AB **15**, 011001 (2012).
- [2] M. Ikegami, PTEP **2012**, 02B002 (2012).
- [3] H. Hotchi et al., PRST-AB **12**, 040402 (2009).
- [4] H. Hotchi et al., PTEP **2012**, 02B003 (2012).
- [5] T. Koseki, Proc. of IPAC14, THPME061.
- [6] M. Kinsho, Proc. of IPAC14, THPME064.
- [7] H. Hotchi et al., PRST-AB **12**, 040402 (2009).
- [8] F. Tamura et al., PRST-AB **12**, 041001 (2009).
- [9] M. Yamamoto et al., NIM, A **621**, 15 (2010).
- [10] Y. Shobuda et al., PRST-AB **12**, 032401 (2009).
- [11] T. Takayanagi et al., Proc. of IPAC12, THPPD051.